HHS Public Access

Author manuscript

Precis Nanomed. Author manuscript; available in PMC 2019 June 27.

Published in final edited form as:

Precis Nanomed. 2018 July ; 1(2): 128–145. doi:10.33218/prnano1(2).180724.1.

Cellular Trafficking of Sn-2 Phosphatidylcholine Prodrugs Studied with Fluorescence Lifetime Imaging and Super-resolution Microscopy

Dolonchampa Maji, PhD[a,b,*], **Jin Lu, PhD**[c], **Pinaki Sarder, Phd**[d], **Anne H. Schmieder, MS**[e], **Grace Cui, MS**[e], **Xiaoxia Yang, BS**[e], **Dipanjan Pan, PhD**[f], **Matthew D. Lew, PhD**[c], **Samuel Achilefu, PhD**[a,b], and **Gregory M. Lanza, MD PhD**[b,e,†]

[a]Optical Radiology Lab, Department of Radiology, Washington University School of Medicine, St. Louis, MO 63110, USA

[b]Department of Biomedical Engineering, Washington University in St. Louis, MO 63130, USA

[c]Department of Electrical and Systems Engineering, Washington University in St. Louis, St. Louis, MO 63130, USA

[d]Department of Pathology and Anatomical Sciences, Jacobs School of Medicine & Biomedical Sciences, University of Buffalo, Buffalo, NY 14203

[e]Division of Cardiology, Department of Medicine, Washington University School of Medicine, St. Louis, MO, USA

[f]Department of Bioengineering, University of Illinois at Urbana-Champaign, Champaign, IL, USA

Abstract

While the *in vivo* efficacy of Sn-2 phosphatidylcholine prodrugs incorporated into targeted, non-pegylated lipid-encapsulated nanoparticles was demonstrated in prior preclinical studies, the microscopic details of cell prodrug internalization and trafficking events are unknown. Classic fluorescence microscopy, fluorescence lifetime imaging microscopy, and single-molecule super-resolution microscopy were used to investigate the cellular handling of doxorubicin-prodrug and AlexaFluor™-488-prodrug. Sn-2 phosphatidylcholine prodrugs delivered by hemifusion of nanoparticle and cell phospholipid membranes functioned as phosphatidylcholine mimics, circumventing the challenges of endosome sequestration and release. Phosphatidylcholine prodrugs in the outer cell membrane leaflet translocated to the inner membrane leaflet by ATP-dependent and ATP-independent mechanisms and distributed broadly within the cytosolic membranes over the next 12 h. A portion of the phosphatidylcholine prodrug populated vesicle membranes trafficked to the perinuclear Golgi/ER region, where the drug was enzymatically liberated and activated. Native doxorubicin entered the cells, passed rapidly to the nucleus, and

[†]Corresponding author: Gregory M. Lanza, M.D. Ph.D. Division of Cardiology, Campus Box 8215, 660 Euclid Ave, Washington University School of Medicine, St. Louis, MO 63108 Tel: 314-454-8813, Fax: 314-454-5265. greg.lanza@mac.com.
[*]Current address Department of Neurological Surgery, Northwestern University, Feinberg School of Medicine, Chicago, IL 60611

Disclosure:
Washington University (GL, DP) has intellectual property rights related to the prodrug technology described in this manuscript. The remaining authors have nothing to disclose.

bound to dsDNA, whereas DOX was first enzymatically liberated from DOX-prodrug within the cytosol, particularly in the perinuclear region, before binding nuclear dsDNA. Much of DOX-prodrug was initially retained within intracellular membranes. *In vitro* anti-proliferation effectiveness of the two drug delivery approaches was equivalent at 48 h, suggesting that residual intracellular DOX-prodrug may constitute a slow-release drug reservoir that enhances effectiveness. We have demonstrated that Sn-2 phosphatidylcholine prodrugs function as phosphatidylcholine mimics following reported pathways of phosphatidylcholine distribution and metabolism. Drug complexed to the Sn-2 fatty acid is enzymatically liberated and reactivated over many hours, which may enhance efficacy overtime.

Graphical Abstract

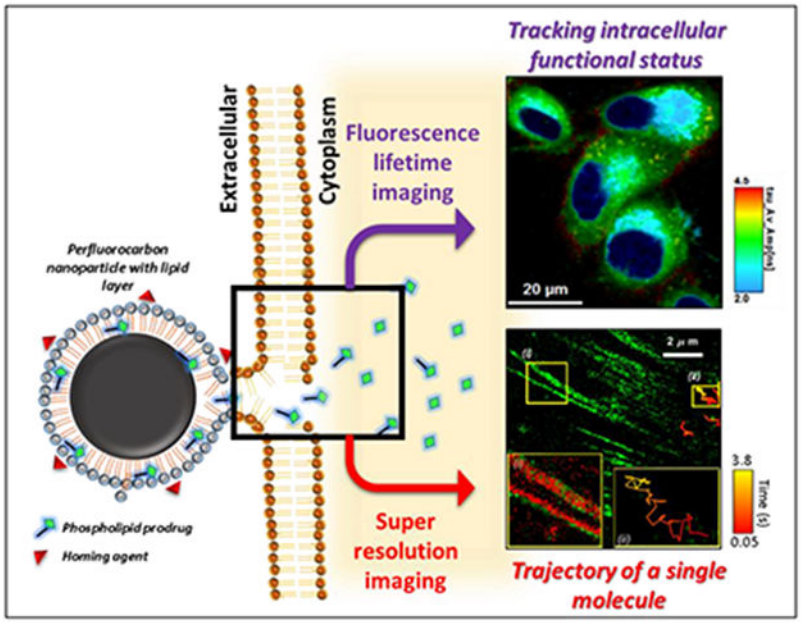

Fluorescence lifetime imaging microscopy (FLIM) and single-molecule super-resolution microscopy (SRM) illustrate the intracellular fate of Sn-2 phosphatidylcholine prodrugs.

Keywords

Phosphatidylcholine prodrugs; Nanomedicine; Fluorescence lifetime imaging microscopy; Super-resolution microscopy

Rationale and purpose

Sn-2 phosphatidylcholine prodrugs in non-pegylated lipid nanoparticle membranes are known to be resistant to premature release and metabolism in circulation. This approach using targeted drug delivery has been demonstrated to be effective in a variety of preclinical models. Cellular uptake of these compounds is hypothesized to be secondary to a hemifusion contact-facilitated drug delivery mechanism with cytosolic enzymatic drug release, which circumvents sequestration in the endosomelysosome pathway. This research

utilized advanced complementary optical imaging methods, including confocal fluorescence lifetime and super-resolution single molecule microscopy, to elucidate and compare PC prodrug cellular trafficking and metabolism with previously known paths of natural PC.

Introduction

The concept of achieving Paul Erhlich's inspired vision of a "magic bullet" to treat disease remains challenging in the context of nanomedicine. While specific reasons vary among nanosystems, in general, early systemic drug loss, low net drug delivery to targeted cells, and limited free drug intracellular bioavailability have been major barriers [1]. Very hydrophobic drugs, such as fumagillin, incorporated into the phosphatidylcholine-based surfactant membranes of $\alpha_v\beta_3$-targeted nanosized emulsion particles [2–7] provided anti-angiogenic benefits that were broadly demonstrated *in vitro* and *in vivo* by imaging, microscopy, and functional outcomes [3, 6–8]. Hydrophobic drugs dissolved into the lipid surfactant spontaneously transferred to targeted cell membranes through an irreversible hemifusion process referred to as contact-facilitated drug delivery (CFDD) [2, 4]. Despite *in vivo* effectiveness, the pharmacokinetics of the drug relative to the other lipid surfactant components and the perfluorocarbon (PFC) core were discrepant and showed marked premature fumagillin loss during circulation [9]. Lipid-anchored homing ligands and gadolinium chelates co-incorporated into the surfactant of PFC nanoparticles (NP) had similar pharmacokinetic clearance rates as a percentage of injected dose in rodents. Fess hydrophobic drugs dissolved into the lipid surfactant, such as paclitaxel or doxorubicin, had rapid circulatory clearance rates compared to the PFC NP core and other membrane constituents. The very poor particle retention of these drugs accounted for their lack of efficacy in cancer models when studied *in vivo* [10].

In an earlier report, rhodamine-PE was employed as a fluorescent drug surrogate to illustrate and elucidate the CFDD mechanism. Rhodamine-PE delivered with integrin-targeted PFC NP integrated into the cell membrane upon binding and readily passed via lipid rafts into C-32 human melanoma cells at 37°C [4]. In contradistinction to rhodamine-PE, paclitaxel conjugated to phosphatidylethanolamine failed to translocate from the outer to inner cell membrane leaflets. The concept of chemically coupling drugs to the Sn-2 fatty acid of phosphatidylcholine (PC) was envisioned as an alternative approach to facilitate nanoparticle drug retention during circulation, to protect chemically-sensitive compounds from interactions with blood constituents, and to transfer into the targeted cell via CFDD. *In vivo* studies demonstrated that the Sn-2 prodrug motif was efficacious for fumagillin, docetaxel, and recently cMYC-inhibitors [9–12].

While the concept of Sn-2 phospholipid prodrugs was never considered for ligand-targeted drug delivery in association with the CFDD hemifusion mechanism, precedence for Sn-2 phospholipid prodrugs was found to exist, initially reported by David Thompson *et al.* in the context of triggered drug release mechanisms [13], Eater, Andresen and colleagues [14–24] pursued an approach to deliver chemotherapeutics as Sn-2 prodrugs via untargeted liposomes, anticipating that phospholipases liberated locally by cancers would trigger local drug release. Their hypothesis was essentially incorrect. Physical-chemical modeling by this team revealed that non-pegylated liposomes were resistant to free water penetration and

premature hydrolysis of the synthetic ether-lipid prodrugs. However, pegylation of liposomes, a design feature commonly employed to extend circulatory half-life, wicked water into the membrane creating access to lipases with resultant rapid premature drug release.

Phosphatidylcholine (PC) populates all cell and intracellular membranes in contrast to phosphatidylethanolamine or phosphatidylserine, which preferentially reside in the inner cell membrane leaflet and other specific organelles, such as the mitochondria [25, 26]. The Sn-2 PC prodrug motif was adopted as a PC mimic that would circumvent endosomal NP internalization and resultant losses by intercalation into the cell membrane and trafficking throughout the intracellular membranes until lipases, such as phospholipase A2, liberated a bioactive drug. However, this working hypothesis for the effectiveness of Sn-2 PC prodrug has never been elucidated.

In the present study, complementary microscopic imaging techniques were utilized to explore cell membrane uptake, cellular internalization and intracellular distribution of a doxorubicin Sn-2 PC prodrug or AlexaFluor™ Sn-2 PC prodrug. The objectives were to compare the biopotency of a phosphatidylcholine doxorubicin prodrug (DOX-PD) with free doxorubicin (DOX) and to utilize fluorescence lifetime imaging microscopy (FLIM) to compare the trafficking of DOX-PD versus free DOX from the outer cell membrane to the nucleus. To corroborate and extend the FLIM results, single-molecule super-resolution optical microscopy [27–29] was employed to map Sn-2 AlexaFluor™ 488 prodrug (AF488-PD) trajectories from the cell membrane uptake, outer to inner membrane leaflet transfer, and throughout the intracellular membranes.

Experimental design

The present study employed traditional fluorescence microscopy, confocal fluorescence lifetime imaging microscopy (FLIM), and single molecule super-resolution optical microscopy in a complementary fashion to track optically active Sn-2 phosphatidylcholine prodrug in normal and cancerous cells. The experimental protocols utilized a doxorubicin prodrug for fluorescence microscopy and confocal fluorescence lifetime imaging for assessments of the cell membrane, cytosol, and nucleus. A more photostable dye, AlexaFluor™ 488, was synthesized into an Sn-2 prodrug motif to detect single prodrug molecules in the presence of autofluorescence. This enhanced photostability extended the SRM tracking time and permitted better estimates of molecular migration patterns and prodrug membrane retention.

Fluorescence microscopy differentiated free DOX and DOX-PD distribution from the outer cell membrane, cytoplasm and nucleus. FLIM, which assessed distributions between local biochemical environments based on changes in excited-state lifetimes, offered qualitative discrimination between drug retained in cell membranes, enzymatically released into the cytosol, or in the nucleus bound to dsDNA. Super-resolution optical microscopy dynamically tracked single prodrug (AF488-PD) molecules across multiple focal planes, demonstrating spatial uptake, translocation and distribution within the cell until the dye was enzymatically liberated, after which rapid molecular motion beyond the confocal volume

precluded detection. Collectively, these observations and measurements demonstrate the CFDD drug delivery mechanism of PC prodrugs and the avoidance of endosomal sequestration and degradation.

Materials and methods

Synthesis and characterization of doxorubicin and AlexaFluor™ 488 prodrugs

Doxorubicin Sn-2 prodrug conjugates (DOX-PD) were synthesized in our laboratory starting from commercially available doxorubicin (Sigma Aldrich, St. Louis, MO) and oxidized phospholipids (NOF America, White Plains, NY). In this approach, doxorubicin (0.22 mM) was dissolved in dimethylsulfoxide (DMSO) and triethylamine (1 mM). Added to this solution was (S)-2-(8-carboxyoctanoyloxy)-3-(palmitoyloxy)propyl 2-(trimethylammonio)ethylphosphate (PAzPC, 0.2 mM, NOF America) dissolved in chloroform with cyclohexylcarbodiimide (1 mM). The reagent mixture was shaken overnight at room temperature (RT) then purified using silica gel column chromatography. The desired product DOX-PD was characterized using mass spectroscopy: Chemical Formula: $C_{60}H_{91}N_2O_{20}P$, ESI-MS $M+H^+$ Cal. 1190.63, exp. 1191.6 (Shimadzu LCMS 2010A, Kyoto, Japan) (Figure S1).

The AlexaFluor™ 488 Sn-2 phospholipid conjugate (AF488-PD) was synthesized from commercially available AlexaFluor™ 488 (Thermo Fisher Scientific, Waltham, MA) and oxidized phosphatidylcholine (NOF America, PAzPC). In this approach, AlexaFluor™ 488 cadaverine (1.56 μmoles in 1 mL dimethylformamide) was combined with excess PAzPC (6.6 pmole) dissolved in 2 mL chloroform to which triethylamine (50 μl) and *N,N'*-diisopropylcarbodiimide (50 μl) were added. The mixture was reacted for 2-3 hours. Separation with silica TLC (0.2M NH_4Ac:MeOH:water - 20:100:200) revealed only the conjugated dye (RF 0); the free dye control was seen at RF ~ 0.8. The sample was dialyzed (MWCO 500-1000) then lyophilized. Purified AF488-PD was characterized using mass spectroscopy: final chemical formula was $C_{74}H_{113}N_7NaO_{23}PS_2+2H^+$, ESI-MS $M+H^+$ Cal. 793, exp.793.85 (Shimadzu LCMS 2010A, Kyoto, Japan) (Figure S1).

Synthesis and characterization of αvβ3 DOX-PD PFOB nanoparticles

Nanoparticles (NP) were prepared as a microfluidized suspension of 20% (v/v) perfluoro-1-bromooctane (PFOB, Exfluor Research Corporation, TX), 2.0% (w/v) of a surfactant co-mixture and 1.7% (w/v) glycerin in Milli-Q® water. An $\alpha_v\beta_3$-integrin antagonist, a quinolone nonpeptide developed by Bristol-Myers Squibb Medical Imaging (US patent US 6511648 and related patents) was used for homing (a gift, Kereos, Inc., St. Louis, MO). The surfactant co-mixture included: approximately 97.6 mole% lecithin, 0.15 mole% of $\alpha_v\beta_3$-ligand-conjugated lipid and 2.28 mole% of DOX-PD (0.5 mM). The surfactant components were combined with the PFOB, buffer and glycerine and Milli-Q® water, then the mixture was homogenized at 20000 psi for 4 min. The NP were preserved under inert gas in sterile sealed vials until use. Nominal $\alpha_v\beta_3$-DOX-PD PFOB NP and size by dynamic light scattering was 260 nm, with a polydispersity of 0.14 and zeta potential of −7.4 mV. The surfactants of fluorescent PFOB NP incorporated 0.1 mol% rhodamine-

phosphatidylethanolamine (Avanti Polar Lipids, Alabaster, AL) or 0.1 mol% AF488-PD in the lipid commixture at the expense of phosphatidylcholine.

Absorption and fluorescence spectroscopy

DOX and DOX-PD were used for absorption and fluorescence spectroscopy. The materials were diluted in Milli-Q® water. Absorption spectra were measured on a DU 640 spectrophotometer (Beckman-Coulter, Brea, CA). Fluorescence emission spectra were recorded on a FluoroLog 3 spectrofluorometer (Horiba Jobin Yvon, Edison, NJ) using 585 nm/600-700 nm as excitation/emission wavelength with 5 nm slits.

Cell culture

For fluorescence microscopy, 2F2B mouse endothelial cells (ATCC CRL2168, Manassas, VA, USA) were cultured in Dulbecco's modified Eagle's medium (DMEM, no phenol red, Gibco, Thermo Fisher Scientific, Waltham, MA) with 4.5 g/L glucose and 10% heat inactivated fetal bovine serum. Cells were plated on sterile 12 mm cover glasses (#1.5) in a 24 well plate at approximately 1×10^5 cells per well and incubated overnight at 37 °C in a 5% CO_2 incubator. Doxorubicin (Sigma, St Louis, MO, USA) or $\alpha_v\beta_3$-DOX-PD PFOB NPs were added to the cells at a final concentration of 3 μM active drug in complete media. After 1 h, the cells were washed three times in PBS and fixed in 4% paraformaldehyde solution for 30 min. The coverslips were rinsed in PBS; the cell nuclei were stained blue with DAPI (4′, 6-diamidino-2-phenylindole, dihydrochloride); and samples were analyzed by fluorescence microscopy (Olympus BX61, Shinjuku, Tokyo, Japan).

For confocal fluorescence lifetime imaging microscopy, human C-32 melanoma cells (Washington University Tissue Culture Support Center, St. Louis, MO) were cultured in Minimal Essential Media containing Earle's salts (no phenol red, Gibco, Thermo Fisher Scientific, Waltham, MA) and supplemented with 10% (v/v) fetal bovine serum (Sigma-Aldrich, St. Louis, MO), 1% penicillin and 1% streptomycin (Gibco). The cells were trypsinized and plated on glass bottom dishes (35 mm, glass #1, MatTek Corporation, Ashland, MA) and grown overnight in phenol red-free media. The drug formulations were diluted in the culture media and cells were incubated for varying times. After incubation and washing, fluorescence lifetime imaging was performed on live cells in a humidified stage-top incubator with 5% CO_2.

For super-resolution imaging, 2F2B mouse endothelial cells were cultured in DMEM with 10% fetal bovine serum (Gibco) plus 1% penicillin and 1% streptomycin (Gibco) and incubated at 37°C with 5% CO_2. 2F2B cells were trypsinized and plated on ozone-pretreated high-tolerance coverslips (No. 1.5, 170 ± 5 μm thickness, Azer Scientific, Morgantown, PA), and incubated for 48 h. The cells were further treated with 1.6 μg/mL AF488-PD at 37 °C for 12 h, or 0.05 μg/mL AF488-PD at room temperature for 5 min before imaging. The 2F2B cells were also treated with 1.4 μM PE-rhodamine at 37 °C for 1 h and rinsed with PBS for standard epifluorescence imaging.

Cytotoxicity assay

The retained cytotoxicity of DOX-PD was compared to native DOX in mouse endothelial cells. 2F2B cells were seeded on a 96 well plate (2000-5000 cells/well) in DMEM with 10% heat-inactivated fetal bovine serum plus 10 μM angiotensin II (Sigma-Aldrich, St. Louis, MO) then incubated at 37 °C with 5% CO_2. After 24 h, cells were incubated for 1 h with a) $\alpha_v\beta_3$-DOX-PD PFOB NP (0.3 μM DOX PD), b) equimolar equivalent of native doxorubicin HC1 or c) $\alpha_v\beta_3$-No drug NP. After incubation the wells were washed three times with PBS and returned to the incubator for 48 h. Cell proliferation was measured using the MTT assay for cytotoxicity, which measures the activity of cellular enzymes that reduce the tetrazolium dye to the insoluble formazan (Invitrogen; Thermo-Fisher Scientific, Waltham, MA). Each treatment was replicated 6 times.

Fluorescence lifetime spectroscopy, imaging and data analysis

Confocal fluorescence lifetime spectroscopy and imaging was performed with a MicroTime 200 microscope (Picoquant, Berlin, Germany). For spectroscopy, fluorescence lifetimes of DOX (50 μM) and DOX-PD (50 μM) solutions in MilliQ® water (final DMSO 0.5%) were measured under a 100× oil immersion objective with 485 nm (15 au) laser excitation pulsed at 40 MHz. Decay data were collected through a 519 nm long pass filter and accumulated until peak photon counts reached 10,000. Almost identical conditions were applied for $\alpha_v\beta_3$-DOX-PD PFOB NPs (25 μM doxorubicin concentration) except the pulse rate was reduced to 20 MHz in order to capture its slower decay. Live cell imaging utilized 485 nm laser excitation (~1000 au) at 20 MHz on cells maintained in a stage top CO_2 incubator for the period of imaging.

Lifetime decay data collected from spectroscopy and microscopic imaging were analyzed on the SymphoTime software (Picoquant, Berlin, Germany). All decays were fit using multi-exponential tail fit using the equation below:

$$y(t) = \sum_{i=0}^{n-1} A[i]\exp\{-\frac{t}{\tau[i]}\} + Bkgr \quad \text{Equation 1}$$

Where: n = number of exponentials (n ≤ 2 for all cases depending on goodness of fit): A = amplitudes: τ = lifetimes: Bkgr = correction for background (after-pulsing, dark counts, environmental light).

Spectroscopy data were fit to mono- or biexponential decay fits (depending on goodness of fit). For cell images, raw decay data from all cellular pixels were fit to bi-exponential models and this method was used to generate the corresponding lifetime images.

For cell compartment specific analyses, nuclear, perinuclear and extra-perinuclear regions of interest (ROIs) were drawn to achieve 1000 or more counts to ensure effective bi-exponential decay analysis. Bi-exponential tail fit was used to fit decays from each ROI and individual components (lifetime and amplitude) were obtained. Good χ^2 values (0.8-1.2) and random distribution of x-axis residuals were considered necessary for an accurate decay

fit. Amplitude average fluorescence lifetimes (τ_{amp}) were calculated and reported using the following model and reported as average lifetime values.

$$\tau_{amp} = \sum_{k=0}^{n-1} A[k]\tau[k] \Big/ \sum_{k=0}^{n-1} A[k] \quad \text{Equation 2}$$

Analyzed data was plotted using Prism (Graphpad, La Jolla, CA). Wherever required, appropriate statistical analysis was performed using Prism's built-in functions and corresponding *p* values were reported.

Super-resolution imaging and data analysis

Single-molecule super-resolution imaging was used to image the binding and cellular uptake of individual prodrug molecules. First, images of individual fluorescent molecules with switchable bright-dark states (blinking) were captured, and their positions were measured by fitting each blinking event to a two-dimensional Gaussian function. A super-resolved image was then reconstructed by combining all positions from the stochastic blinking events of fluorescent molecules. To resolve the fluorescence signal from a single molecule, a bright fluorophore, AlexaFluor™ 488 (AF488), was used and conjugated to the phospholipid at the Sn-2 position as the prodrug analog for super-resolution imaging. AF488-PD was more photostable than DOX-PD and permitted detection of single copies of AF488-PD in the presence of autofluorescence, extending SRM tracking time and improving estimates of molecular migration patterns and prodrug membrane retention. Freely-diffusing AF488-PD in the extracellular buffer and in the cytosol were not captured, since their quickly-moving fluorescence signals were out of focus and/or averaged out by the detector. However, when AF488-PD temporarily docked onto the lipid membrane, its slowed diffusion was captured and localized from which a superresolution image was reconstructed with spatial resolution beyond refraction limit. In this way, single-molecule super-resolution imaging precisely localized the prodrug molecules with single-molecule sensitivity.

Super-resolution imaging was performed on a home-built microscope equipped with a 100X oil immersion objective (Figure S2) [30, 31]. After AF488-PD incubation, the cells were washed with PBS to remove the excess prodrug in the media. Cells were first illuminated with a 488-nm laser (OBIS, Coherent) at a peak intensity of 0.12 kW/cm^2 at the sample. The images were filtered with a 523/610 dual-band bandpass filter (Semrock FFO1-523/610) and acquired by a sCMOS camera (Hamamatsu, C11440-22CU) with a 50 ms exposure time. Next, merocyanine 540 (MC540, Invitrogen) was introduced to cell media to image the cell membranes via PAINT (Point Accumulation for Imaging in Nanoscale Topography) [32]. Similar to AF488-PD, localizations were only acquired when MC540 temporarily docked with the cell membranes and emitted bright fluorescence, thereby enabling the colocalization of prodrug molecules relative to cell membrane with nanoscale resolution. MC540 was excited with a 561-nm laser (Sapphire, Coherent) at a peak intensity of 2.7 kW/cnf at the sample, and images were acquired with a 50 ms exposure time. The single AF488-PD and MC540 molecules were identified and localized by two-dimensional Gaussian fitting using an ImageJ plug-in ThunderSTORM [33].

The super-resolution images of prodrug and cell membranes consist of the sum of all localizations from AF488-PD and MC540 respectively, binned as a 2D histogram with bin size 58.5×58.5 nm^2. AF488-PD localizations over time were grouped into a trajectory when present in consecutive frames (up to a 3-frame gap) within a distance of 0.59 μm. The trajectories were plotted using custom software (MATLAB, MathWorks). No trajectory analysis was performed for the endothelial filopodia.

Results

Spectroscopic characterization of synthesized prodrugs

Absorption and fluorescence spectra and decay characteristics of the materials were measured in a water solution. DOX and DOX-PD had similar absorption spectra (Figure 1A). The spectra for $\alpha_v\beta_3$-DOX-PD PFOB NP was obscured by light scattering.

All drug formulations showed similar fluorescence emission spectra, which corroborated the presence of doxorubicin in the nanoparticles (Figure 1B). The emission peak at ~556 nm for doxorubicin in the $\alpha_v\beta_3$-DOX PFOB NP was relatively more prominent. This observation may reflect the unique interactions of the doxorubicin molecules with the core PFOB molecules that penetrate to the particle-water interface [34].

As shown in Figure 1C, free DOX fluorescence fit a mono-exponential decay of 1.09 ± 0.02 ns ($\chi 2 = 1.06$), consistent with literature findings. DOX-PD decay best fit a biexponential decay model with nearly equal contributions from a fast lifetime component $\tau_a = 0.69 \pm 0.06$ ns (53%) and a slow lifetime component of $\tau_b = 1.21 \pm 0.03$ ns (47%), indicative of a heterogeneous system ($\chi 2 = 1.007$). The amplitude average lifetime (τ_{amp}) was calculated to be 0.96 ± 0.04 ns. Dynamic light scattering analysis of a DOX-PD in water revealed a mixed suspension of free prodrug molecules and spontaneously formed prodrug micelle aggregates (~1600 nm). Fluorescence lifetime of doxorubicin bound to biological molecules (lipid membranes, DNA) and while encapsulated in nanoparticles increases as the molecules are shielded from external fluorescence quenchers and by π-π stacking [35–38]. Hence, the slower lifetime component from DOX-PD suspension was attributed to the micellar fraction of the drug distribution where the anthracycline portion of DOX-PD was shielded from surrounding water molecules. The faster lifetime of 0.69 ns can be attributed to the free DOX-PD molecules in water. This value is slightly different than that of free DOX in water, reflecting the effect of drug conjugation with the lipid molecule. Fluorescence decay of $\alpha_v\beta_3$-DOX-PD PFOB NP fit a double exponential decay model with components $\tau_a = 3.78 \pm 0.03$ ns (22%) and $\tau_b = 1.34$ ns (78%) ($\chi^2 = 1.03$). The majority of the $\alpha_v\beta_3$-DOX-PD PFOB NP had the faster fluorescence lifetime component (1.34 ns) similar to that of DOX-PD in the micellar fraction (1.21), indicating similar hydrophobic interactions. The slower lifetime fractional component (3.78 ns) is likely related to hydrophobic interactions of DOX-PD within the nanoparticle lipid surfactant intercalated between PFOB molecules.

Cellular uptake and cytotoxicity of αvβ3-DOX-PD PFOB NP

The cellular distribution of DOX presented as the free drug and delivered within nanoparticle surfactant in prodrug form was observed with fluorescence microscopy (Figure 2).

Benign 2F2B mouse endothelial cells were exposed to DOX and $\alpha_v\beta_3$-DOX-PD PFOB NP. Free DOX internalized and localized rapidly to cell nuclei within 30 min of treatment with negligible cytosolic retention noted (Figure 2A). DOX-PD delivered by $\alpha_v\beta_3$-targeted NP bound to the cell membrane periphery, entered the cell via the CFDD mechanism and rapidly dispersed into the cytosol membranes. Lipase-released DOX was observed in the nucleus (Figure 2B). Circumventing cell internalization with endosome sequestration and escape, a common pathway for nanoparticle drug delivery, DOX-PD dispersed throughout the cytoplasmic membrane. Enzymatically liberated DOX accumulated in the nucleus.

The cytotoxic bioactivity of $\alpha_v\beta_3$-targeted DOX-PD PFOB NP referenced to equimolar free DOX was assessed in 2F2B mouse endothelial cells stimulated with angiotensin II using the MTT cytotoxicity assay. The control $\alpha_v\beta_3$-no-drug NP had no impact on cell proliferation (Figure 2C). Both free DOX added to the media and $\alpha_v\beta_3$-DOX-PD PFOB NP were cytotoxic (Figure 2C). At 48 h $\alpha_v\beta_3$-DOX-PD PFOB NP decreased cell proliferation by 44% ($P<0.01$) as compared to the control $\alpha_v\beta_3$-no-drug NP. An equivalent dose of free DOX decreased cell proliferation by 19% ($P<0.05$) compared to the control. The $\alpha_v\beta_3$-DOX-PD PFOB NP was significantly more toxic than equivalent amounts of free DOX ($P<0.05$). These data showed that the Sn-2 coupling of DOX to the phosphatidylcholine lipid backbone did not compromise drug net bioactivity and suggested that continued liberation of DOX from the DOX-PD reservoir retained in the cytoplasm over 48 hours contributed to effectiveness.

Temperature dependent cellular uptake of αvβ3-DOX-PD PFOB NP

Fluorescence imaging of prodrug trafficking performed in normal proliferating endothelial cells was reflective of previous anti angiogenesis experiments [10, 12, 39, 40] with Sn-2 prodrugs. As opposed to normal proliferating endothelial cells, the next experiments explored Sn-2 prodrug behavior in abnormal human C-32 melanoma.

Drug uptake from $\alpha_v\beta_3$-DOX-PD PFOB NP was studied in cultured C-32 cells at 37 °C and at 4 °C, the later to induce cold suppression of ATP-dependent mechanisms (Figure 3).

DOX-PD transfer from the bound nanoparticle surfactant to the outer cell membrane leaflets was similar under both temperature regimens. While transfer of DOX-PD from the outer to inner cell membrane leaflets was rapid and unimpaired at 37 °C, at 4 °C DOX-PD delivery to the inner leaflet and contiguous intracellular membranes was reduced but notably present well-above background fluorescence. This was in contradistinction to previous studies using rhodamine-PE as a drug surrogate in which translocation of the fluorescent lipid from the outer to inner cell membrane leaflets was blocked at 4 °C. These data suggest that DOX-PD and other PC-PD will translocate between membrane leaflets by ATP-dependent and ATP-independent mechanisms and slowly diffuse into cells in the absence of energy.

Pixel-by-pixel fit of the raw decay data shows gradient of amplitude average lifetime r_{amp} throughout the cells (Figure 4B). Untreated cells showed minimal background signal under these imaging conditions (Figure S4). We performed cell compartment specific analysis of our lifetime data as below (Figure S5).

Nucleus

Nuclei of cells treated with DOX and $\alpha_v\beta_3$-DOX-PD PFOB-NPs showed similar lifetime distribution suggesting that DOX liberated from lipid prodrug retained the same dsDNA binding character as the native compound (Figure S3). Previous studies have reported DOX bound to dsDNA exhibits higher lifetime (2.2 ns – 1.3 ns, [37, 38, 41]). Upon fitting decays from nuclear ROIs using bi-exponential model, a major component of fast lifetime 1.44 ns ± 0.06 ns (80% ± 4%, n=52) was detected reflecting dsDNA-bound DOX. A minor slow lifetime component (3.80 ± 0.24 ns) in the nucleus was attributed to noise from backscattering of excitation light and autofluorescence, which was also noted for untreated cells (Figure S4). $\boldsymbol{\tau}_{amp}$ in the nuclei decreased steadily between 1 h (2.11 ± 0.04 ns) and 8 h (1.82 ± 0.02) post-incubation (Figure 4C, $P<0.001$). This observation was previously observed by others and attributed to drug-induced apoptosis with consequent remodeling of chromatin network in the nucleus [41].

Cytoplasm

The cytoplasm of cells treated with $\alpha_v\beta_3$-DOX-PD PFOB-NPs demonstrated fluorescence signal at all time points with consistently high signal noted in the perinuclear space (Figure 4A, red arrows). This region coincides with the location of Golgi/ER, which is associated with enriched levels of cytosolic phospholipase A2 (cPLA2) activity [42]. Comparisons within and outside the bright perinuclear regions showed lower $\boldsymbol{\tau}_{amp}$ (1.8 ns ± 0.2 ns, n=15 ROI) in the perinuclear regions than the later ($\boldsymbol{\tau}_{amp}$ = 2.9 ns ± 0.3 ns, n= 15 ROI). The lower $\boldsymbol{\tau}_{amp}$ observed in bright perinuclear region was due to greater contribution from a faster lifetime component (1.1 ns, 82% ±3%) suggesting an abundance of free DOX molecules. In the surrounding cytosol, this faster component was much less in proportion (1.06 ns, 52% ± 8%), indicating lower amounts of free DOX (Figure 4D). The slower lifetime components from both perinuclear and surrounding regions was attributed to a combination of background (as observed in cell nuclei) and from bound drug (as observed in literature and our spectroscopic studies). By extension, the collective data suggested that phospholipase release of Sn-2-linked doxorubicin from the PC backbone was more concentrated in the perinuclear region than in the general cytosol.

Super-resolution microscopy of cellular binding and internalization of prodrug molecules

Single-molecule super-resolution microscopy (SRM) captures images of fluorescent molecules with nanometer resolution beyond the optical diffraction limit. The AF488-PD, which contains fluorescent AF488 molecules conjugated to the phospholipid at the Sn-2 position, preferentially intercalated into the outer membrane leaflet of cells.

In 2F2B endothelial cells, AF488-PD (Figure 5A, red) was imaged within the cell membrane after 5 min of incubation, co-localizing with another membrane marker dye, MC540 (Figure 5A, green). As noted in the bright field images shown in Figure 5A, SRM of AF488-PD and

MC540 both accumulated in the outer cell membrane at different z heights (1, 2, 3 μm) above the coverslip. These merged PAINT images suggested that the PC prodrug inherently incorporated into the cell membrane with little spatial restriction between the base of the cell on the coverslip and the apical surface fully exposed to the bulk media. In addition to the primary cell body surface membrane, AF488-PD also incorporated into 2F2B cell filopodia processes as noted in the magnified image of the box (i) in Figure 5B. In contradistinction, standard epifluorescence microscopy imaging showed that the PE-rhodamine did not broadly intercalate into the outer phospholipid cell membrane but was primarily associated with the cell along the coverslip region where cell adherent molecules are highly expressed and engaged (Figure S6). This observation was consistent with the report of Partlow et al, which associated PE-rhodamine uptake with specific lipid-raft membrane regions [4].

The diffusion of single molecules of AF488-PD through the cytosol was imaged using single-molecule fluorescence imaging (Supplementary video S1). The trajectories shown in Figure 5B illustrated the trackable paths of single prodrug molecules prior to photobleaching, diffusion beyond the focal plane of the microscope, or enzymatic dye liberation into the cytosol. Two representative trajectories are presented in the magnified images, box (ii) and (iii), in Figure 5B. Individual freely-diffusing prodrug molecules were also observed at the coverslip level of the cell, which likely reflected the rapid mobility of cell membrane phospholipid constituents [43].

With longer incubation times at 37 °C more AF488-PD entered the membrane from the media and internalized into the cell. Figure 5C shows the fluorescence images of 2F2B cells after incubation with AF488-PD for 12 h. At this stage, AF488 fluorophores accumulated broadly within the internal cell membranes particularly in the perinuclear region, corroborating the fluorescence microscopy observation. Fluorescence images obtained at different z heights (Figure 5C at 0.5, 2.5, 6.5 μm above the coverslip) showed dye throughout the cell with the intensity of the light signal proportional to the proximity of AF488-PD to the microscope's focal plane, while the autofluorescence background from 2F2B cells was low (Figure S7). Diffuse red signal associated with AF488-PD was noted beyond the microscope's depth of field. The rapid motion of freely diffusing liberated AF488 molecules were not resolved in the cytoplasm (Figure 5C).

Discussion

In vivo efficacy of Sn-2 PC prodrugs incorporated into the surfactant of lipid-encapsulated nanoparticles has been demonstrated previously [9–12]. These studies showed that the Sn-2 PC PD motif inhibited significant premature drug loss and drug metabolism during circulation to the targeted pathology. However, evidence corroborating prodrug avoidance of internalization and sequestration within the endosome/lysosome pathway versus CFDD-mediated translocation into intracellular membrane distribution with subsequent enzymatic drug liberation was lacking. In the present series of experiments, PC prodrug delivery into cells and intracellular trafficking was investigated using three complementary optical imaging methods: classic fluorescence microscopy, fluorescence lifetime imaging microscopy, and singlemolecule super-resolution microscopy. The overarching result suggests that the PC prodrugs act as mimics of phosphatidylcholine with regard to cell

membrane uptake, membrane leaflet translocation, intracellular distribution, and enzymatic metabolism in normal and cancerous cell lines.

In prior research with rhodamine-PE as a lipid drug surrogate in $\alpha_v\beta_3$-targeted lipid-encapsulated NP, access into cells was confined to lipid rafts and transfer of the fluorescent PE from the outer to inner cell membrane leaflets was dependent on ATP, consistent with the a well-known amino-phospholipid flippase transport protein mechanism. In ATP-starved situations, such as hypoxic cancer cells, targeted delivery of PE-based prodrugs could be compromised. In contradistinction, PC-prodrugs intercalated throughout the outer cell membrane leaflet, including filopodia processes and translocated to the inner leaflet rapidly at 37 °C. ATP-suppressing cold treatment (4 °C) partially inhibited the outer to inner membrane leaflet translocation of PC-prodrug, but substantial drug transferred into the inner leaflet and then migrated throughout the cytosolic membranes. These data suggest that DOX-PD and other PC-PD will translocate between membrane leaflets by ATP-dependent and ATP-independent mechanisms and slowly diffuse into cells in the absence of energy. Moreover, spatially unrestricted cell entry combined with ATP independent translocation into the cell are both favorable for drug delivery.

PC prodrugs broadly disseminated into cytosolic membranes overtime, but a significant intracellular trajectory was noted in the lipid membranes of vesicles, likely endosomes, trafficking toward the perinuclear nuclear Golgi/ER region, a pathway well-documented for native PC [26]. The perinuclear Golgi/ER region has enriched concentrations of cytoplasmic phospholipase A2, a lipase involved in the degradation and recycling of phosphatidylcholine [42, 44]. Enhanced local perinuclear enzymatic liberation was demonstrated with doxorubicin Sn-2 prodrug (DOX-PD) and fluorescence lifetime microscopy. In perinuclear Golgi/ER region, increased concentrations of free doxorubicin were estimated. In other cytoplasmic membrane regions with prevalent DOX-PD retention, substantially lower concentrations of released drug were estimated.

Fluorescence lifetime imaging further demonstrated that the PC-released doxorubicin entered the nucleus and bound to dsDNA similar to native doxorubicin. In culture, free doxorubicin entered cells rapidly and localized to the nucleus with negligible cytoplasm retention. By comparison, DOX-PD entered the cell after NP targeting and a visually significant portion of the drug rapidly bound within the nucleus. However, unlike free DOX, less drug was observed in the nucleus and a significant proportion of the prodrug remained within the cytoplasmic membranes. Nevertheless, the biopotency of the native and prodrugs were at least equivalent with regard to cell proliferation when measured by MTT assay at 48 hours. If the drug cytotoxicity is directly correlated to the compound bound to dsDNA, then the residual prodrug within the intracellular membrane may have constituted a slower release depot with continued drug liberated over the 48-hour experiment increasing nuclear DOX delivery. Alternatively, the slower translocation of DOX-PD to the nucleus with residual cytoplasm retention may have increased the antiproliferative contributions of other pathways of doxorubicin toxicity, such as in the mitochondria [45].

In the present study, definitive confirmation of PC-PD migration to the Golgi, specifically, was not established and tracking to the endoplasmic reticulum or both organelles in the

perinuclear region could not be differentiated. Additionally, the potential role of doxorubicin exocytosis when delivered as the prodrug versus free drug form was not studied. Attention was placed on the binding of liberated DOX to DNA over time, which evolved slowly from the retained cytosol membrane depot. Finally, the MTT assay was used to assess cell apoptosis. Although careful washing of residual doxorubicin prior to the addition of assay reagents to the cell culture was performed, a complementary caspase assay might additionally inform whether the treated cells cycled into apoptosis versus the control.

Conclusion

Sn-2 lipase labile phospholipid prodrugs in combination with the contact-facilitated drug delivery mechanism have been demonstrated for targeted nanoparticle therapy in vivo. In this report, traditional fluorescence microscopy, fluorescence lifetime imaging, and single-molecule super¬resolution imaging techniques were used to elucidate the intracellular trafficking and metabolism details of PC prodrugs for the first time. PC prodrugs incorporated broadly into the outer cell membrane leaflet over the cell body and filopodia, and translocated to the inner membrane leaflet by ATP-dependent and ATP-independent mechanisms. Nanoparticles were not sequestered into endosomal vesicles, but the PC prodrugs delivered into the cells populated vesicle membranes that trafficked to the perinuclear Golgi/ER region as well as distributed through the intracellular membranes in the cytosol. As an example, doxorubicin-prodrug tracked to the Golgi/ER region where the highest level of liberated drug was measured compared to the general cytosol. The released anthracycline displayed similar fluorescence lifetimes when bound to dsDNA as the native. In contradistinction to free doxorubicin, which transferred directly to the nucleus after cell uptake, a significant portion of DOX-PD remained within cytosolic membranes. Nevertheless, the biopotency of the native and prodrugs were at least equivalent with regard to cell proliferation at 48 h, which suggests that the retained DOX-PD may have constituted a prolonged release reservoir that enhanced effectiveness over two days. While the specific fluorescence lifetimes measured in the present study have limited relationship with values for *in vivo* imaging, this study provided the first evidence-based understanding of intracellular Sn-2 PC prodrug fate.

Supplementary Material

Refer to Web version on PubMed Central for supplementary material.

Acknowledgements

Partial funding support was received from the Bames-Jewish Hospital Research Foundation, St Louis, MO, 63110 and from the NIH: HL122471, HHSN-268201400042C, HL112518, HL112518, HL113392, CA199092, CA154737, S10 OD016237, P50CA094056. DM was supported by the Imaging Sciences Pathway graduate student fellowship at Washington University in St. Louis under grant number NIH T32 EB014855.

Abbreviations:

AF488	AlexaFluor™ 488
API	active pharmaceutical ingredient

$\alpha_v\beta_3$	alpha v beta 3 integrin
CFDD	Contact Facilitated Drug Delivery
cPLA2	cytosolic phospholipase A2
DAPI	4′,6-Diamidino-2-phenylindole, dihydrochloride
DMEM	Dulbecco's Modified Eagle's Medium
dsDNA	double-stranded deoxyribonucleic acid
ER	endoplasmic reticulum
FLIM	fluorescence lifetime imaging microscopy
MC540	merocyanine 540
PAINT	Point Accumulation for Imaging in Nanoscale Topography
Paz-PC	1-palmitoyl-2-azelaoyl-sn-glycero-3-phosphocholine"
PC	phosphatidylcholine
PD	prodrug
PFOB	perfluoro-1-bromooctane
PE	phosphatidylethanolamine
PE-PTX	phosphatidylethanolamine-paclitaxel
PLA	phospholipase
SRM	super-resolution microscopy
Sn-2	stereospecific numbering position 2
τ_{amp}	amplitude average lifetime

Bibliography

[1]. Lanza GM, Moonen C, Baker JR Jr., Chang E, Cheng Z, Grodzinski P, Ferrara K, Hynynen K, Kelloff G, Lee YE, Patri AK, Sept D, Schnitzer JE, Wood BJ, Zhang M, Zheng G, and Farahani K, "Assessing the barriers to image-guided drug delivery," Wiley Interdiscip Rev Nanomed Nanobiotechnol, vol. 6, no. 1, pp. 1–14, Jan-Feb, 2014. [PubMed: 24339356]

[2]. Lanza GM, Yu X, Winter PM, Abendschein DR, Karukstis KK, Scott MJ, Chinen LK, Fuhrhop RW, Scherrer DE, and Wickline SA, "Targeted antiproliferative drug delivery to vascular smooth muscle cells with a magnetic resonance imaging nanoparticle contrast agent: implications for rational therapy of restenosis," Circulation, vol. 106, no. 22, pp. 2842–7, 11 26, 2002. [PubMed: 12451012]

[3]. Winter PM, Neubauer AM, Caruthers SD, Harris TD, Robertson JD, Williams TA, Schmieder AH, Hu G, Allen JS, Lacy EK, Zhang H, Wickline SA, and Lanza GM, "Endothelial alpha(v)beta3 integrin-targeted fumagillin nanoparticles inhibit angiogenesis in atherosclerosis," Arterioscler Thromb Vasc Biol, vol. 26, no. 9, pp. 2103–9, 9, 2006. [PubMed: 16825592]

[4]. Partlow KC, Lanza GM, and Wickline SA, “Exploiting lipid raft transport with membrane targeted nanoparticles: a strategy for cytosolic drug delivery,” Biomaterials, vol. 29, no. 23, pp. 3367–75, 8, 2008. [PubMed: 18485474]

[5]. Cyrus T, Zhang H, Allen JS, Williams TA, Hu G, Caruthers SD, Wickline SA, and Lanza GM, “Intramural delivery of rapamycin with alphavbeta3-targeted paramagnetic nanoparticles inhibits stenosis after balloon injury,” Arterioscler Thromb Vasc Biol, vol. 28, no. 5, pp. 820–6, 5, 2008. [PubMed: 18292395]

[6]. Winter PM, Caruthers SD, Zhang H, Williams TA, Wickline SA, and Lanza GM, “Antiangiogenic synergism of integrin-targeted fumagillin nanoparticles and atorvastatin in atherosclerosis,” JACC Cardiovasc Imaging, vol. 1, no. 5, pp. 624–34, 9, 2008. [PubMed: 19356492]

[7]. Zhou HF, Chan HW, Wickline SA, Lanza GM, and Pham CT, “Alphavbeta3-targeted nanotherapy suppresses inflammatory arthritis in mice,” FASEB Journal, vol. 23, no. 9, pp. 2978–85, 9, 2009. [PubMed: 19376816]

[8]. Winter PM, Schmieder AH, Caruthers SD, Keene JL, Zhang H, Wickline SA, and Lanza GM, “Minute dosages of alpha(nu)beta3-targeted fumagillin nanoparticles impair Vx-2 tumor angiogenesis and development in rabbits,” FASEB J, vol. 22, no. 8, pp. 2758–67, 8, 2008. [PubMed: 18362202]

[9]. Pan D, Sanyal N, Schmieder AH, Senpan A, Kim B, Yang X, Hu G, Allen JS, Gross RW, Wickline SA, and Lanza GM, “Antiangiogenic nanotherapy with lipase-labile Sn-2 fumagillin prodrug,” Nanomedicine (Lond), vol. 7, no. 10, pp. 1507–19, 10, 2012. [PubMed: 22709347]

[10]. Pan D, Schmieder AH, Wang KZ, Yang XX, Senpan A, Cui G, Killgore K, Kim B, Allen JS, Zhang HY, Caruthers SD, Shen BZ, Wickline SA, and Lanza GM, “Anti-angiogenesis therapy in the Vx2 rabbit cancer model with a lipase-cleavable Sn-2 taxane phospholipid prodrug using alpha(v)beta(3)-targeted theranostic nanoparticles,” Theranostics, vol. 4, no. 6, pp. 565–578, 2014. [PubMed: 24723979]

[11]. Soodgupta D, Pan D, Cui G, Senpan A, Yang X, Lu L, Weilbaecher KN, Prochownik EV, Lanza GM, and Tomasson MH, “Small molecule MYC inhibitor conjugated to integrin-targeted nanoparticles extends survival in a mouse model of disseminated multiple myeloma,” Mol Cancer Ther, vol. 14, no. 6, pp. 1286–94, 6, 2015. [PubMed: 25824336]

[12]. Zhou HF, Yan H, Hu Y, Springer LE, Yang X, Wickline SA, Pan D, Lanza GM, and Pham CT, “Fumagillin prodrug nanotherapy suppresses macrophage inflammatory response via endothelial nitric oxide,” ACS Nano, vol. 8, no. 7, pp. 7305–17, 7 22, 2014. [PubMed: 24941020]

[13]. Wymer N, Gerasimov O, and Thompson D, “Cascade liposomal triggering: Light-induced Ca2+ release from diplasmenylcholine liposomes triggers PLA2-catalyzed hydrolysis and contents leakage from DPPC liposomes.,” Bioconjug Chem, vol. 9, pp. 305–308, 1998. [PubMed: 9576803]

[14]. Andresen TL, Davidsen J, Begtrup M, Mouritsen OG, and Jørgensen K, “Enzymatic release of antitumor ether lipids by specific phospholipase A2 activation of liposome-forming prodrugs,” J Med Chem, vol. 47, no. 7, pp. 1694–1703, 2004. [PubMed: 15027860]

[15]. Andresen TL, and Jørgensen K, “Synthesis and membrane behavior of a new class of unnatural phospholipid analogs useful as phospholipase A2 degradable liposomal drug carriers,” Biochimica et Biophysica Acta - Biomembranes, vol. 1669, no. 1, pp. 1–7, 2005.

[16]. Andresen TL, Jensen SS, Madsen R, and Jørgensen K, “Synthesis and biological activity of anticancer ether lipids that are specifically released by phospholipase A2 in tumor tissue,” J Med Chem, vol. 48, no. 23, pp. 7305–7314, 2005. [PubMed: 16279790]

[17]. Davidsen J, Jøgensen K, Andresen TL, and Mouritsen OG, “Secreted phospholipase A2 as a new enzymatic trigger mechanism for localised liposomal drug release and absorption in diseased tissue,” Biochim Biophys Acta, Rev Biomembr, vol. 1609, no. 1, pp. 95–101, 2003.

[18]. Jensen SS, Andresen TL, Davidsen J, Høyrup P, Shnyder SD, Bibby MC, Gill JH, and Jørgensen K, “Secretory phospholipase A2 as tumor-specific trigger for targeted delivery of a novel class of liposomal prodrug anticancer etherlipids,” Mol Cancer Ther, vol. 3, no. 11, pp. 1451–1458, 2004. [PubMed: 15542784]

[19]. Kaasgaard T, Andresen TL, Jensen SS, Holte RO, Jensen LT, and Jørgensen K, “Liposomes containing alkylated methotrexate analogues for phospholipase A2 mediated tumor targeted drug delivery,” Chem Phys Lipids, vol. 157, no. 2, pp. 94–103, 2009. [PubMed: 19094974]

[20]. Linderoth L, Peters G, Madsen R, and Andresen T, “Drug delivery by an enzyme-mediated cyclization of a lipid prodrug with unique bilayer-formation properties.,” Angew Chem - Int Edit, vol. 48, pp. 1823–1826, 2009.

[21]. Madsen J, Linderoth L, Subramanian A, Andresen T, and Peters G, “Secretory phospholipase A2 activity toward diverse substrates,” J Phys Chem B, vol. 115, pp. 6853–6861, 2011. [PubMed: 21561115]

[22]. Pedersen P, Adolph S, Subramanian A, Arouri A, Andresen T, Mouritsen O, Madsen R, Madsen M, Peters G, and Clausen M, “Liposomal formulation of retinoids designed for enzyme triggered release. ,” J Med Chem, vol. 53, pp. 3782–3792, 2010. [PubMed: 20405849]

[23]. Pedersen P, Christensen M, Ruysschaert T, Linderoth L, Andresen TL, Melander F, Mouritsen O, Madsen R, and Clausen M, “Synthesis and biophysical characterization of chlorambucil anticancer ether lipid prodrugs,” J Med Chem, vol. 52, pp. 3408–3415, 2009. [PubMed: 19402667]

[24]. Peters G, Møller M, Jørgensen K, Rönnholm P, Mikkelsen M, and Andresen T, “Secretory phospholipase A2 hydrolysis of phospholipid analogues is dependent on water accessibility to the active site,” *J Am Chem Soc* vol. 129, no. 17, pp. 5451–5461, 2007.

[25]. Osman C, Voelker DR, and Langer T, “Making heads or tails of phospholipids in mitochondria,” J Cell Biol, vol. 192, no. 1, pp. 7–16, 1 10, 2011. [PubMed: 21220505]

[26]. Vance JE, “Phospholipid synthesis and transport in mammalian cells,” Traffic, vol. 16, no. 1, pp. 1–18, 1, 2015. [PubMed: 25243850]

[27]. Moerner WE, “Single-molecule spectroscopy, imaging, and photocontrol: foundations for super-resolution microscopy (Nobel lecture),” Angew Chem Int Ed Engl, vol. 54, no. 28, pp. 8067–93, 7 6, 2015. [PubMed: 26088273]

[28]. Hell SW, “Nanoscopy with focused light (Nobel lecture),” Angew Chem Int Ed Engl, vol. 54, no. 28, pp. 8054–66, 7 6, 2015. [PubMed: 26088439]

[29]. Betzig E, “Single molecules, cells, and super-resolution optics (Nobel lecture),” Angew Chem Int Ed Engl, vol. 54, no. 28, pp. 8034–53, 7 6, 2015. [PubMed: 26087684]

[30]. Spehar K, Ding T, Sun Y, Kedia N, Lu J, Nahass GR, Lew MD, and Bieschke J, “Super-resolution imaging of amyloid structures over extended times using Transient binding of single thioflavin T molecules,” Chembiochem, 6 28, 2018.

[31]. Backlund MP, Lew MD, Backer AS, Sahl SJ, Grover G, Agrawal A, Piestun R, and Moerner WE, “Simultaneous, accurate measurement of the 3D position and orientation of single molecules,” Proc Natl Acad Sci U S A, vol. 109, no. 47, pp. 19087–92, 11 20, 2012. [PubMed: 23129640]

[32]. Sharonov A, and Hochstrasser RM, “Wide-field subdiffraction imaging by accumulated binding of diffusing probes,” Proc Natl Acad Sci U S A, vol. 103, no. 50, pp. 18911–6, 12 12, 2006. [PubMed: 17142314]

[33]. Ovesny M, Krizek P, Borkovec J, Svindrych Z, and Hagen GM, “ThunderSTORM: a comprehensive ImageJ plug-in for PALM and STORM data analysis and super-resolution imaging,” Bioinformatics, vol. 30, no. 16, pp. 2389–90, 8 15, 2014. [PubMed: 24771516]

[34]. Lee SJ, Schlesinger PH, Wickline SA, Lanza GM, and Baker NA, “Simulation of fusion-mediated nanoemulsion interactions with model lipid bilayers,” Soft Matter, vol. 8, no. 26, pp. 3024–3035, 1 1, 2012. [PubMed: 22712024]

[35]. Suarasan S, Focsan M, Potara M, Soritau O, Florea A, Maniu D, and Astilean S, “Doxorubicin-incorporated nanotherapeutic delivery system based on gelatin-coated gold nanoparticles: formulation, drug release, and multimodal imaging of cellular internalization,” ACS Appl Mater Interfaces, vol. 8, no. 35, pp. 22900–13, 9 7, 2016. [PubMed: 27537061]

[36]. Dai X, Yue Z, Eccleston ME, Swartling J, Slater NK, and Kaminski CF, “Fluorescence intensity and lifetime imaging of free and micellar-encapsulated doxorubicin in living cells,” Nanomedicine, vol. 4, no. 1, pp. 49–56, 3, 2008. [PubMed: 18249155]

[37]. Zhang X, Shastry S, Bradforth SE, and Nadeau JL, “Nuclear uptake of ultrasmall gold-doxorubicin conjugates imaged by fluorescence lifetime imaging microscopy (FLIM) and electron microscopy,” Nanoscale, vol. 7, no. 1, pp. 240–251, 2015. [PubMed: 25407725]

[38]. Basuki JS, Duong HTT, Macmillan A, Erlich RB, Esser L, Akerfeldt MC, Whan RM, Kavallaris M, Boyer C, and Davis TP, “Using fluorescence lifetime imaging microscopy to monitor

theranostic nanoparticle uptake and intracellular doxorubicin release," ACS Nano, vol. 7, no. 11, pp. 10175–10189, 11, 2013. [PubMed: 24131276]

[39]. Esser AK, Schmieder AH, Ross MH, Xiang J, Su X, Cui G, Zhang H, Yang X, Allen JS, Williams T, Wickline SA, Pan D, Lanza GM, and Weilbaecher KN, "Dual-therapy with alphavbeta3-targeted Sn-2 lipase-labile fumagillin-prodrug nanoparticles and zoledronic acid in the Vx2 rabbit tumor model," Nanomedicine, vol. 12, no. 1, pp. 201–11, 1, 2016. [PubMed: 26515754]

[40]. Zhou HF, Yan HM, Senpan A, Wickline SA, Pan D, Lanza GM, and Pham CTN, "Suppression of inflammation in a mouse model of rheumatoid arthritis using targeted lipase-labile fumagillin prodrug nanoparticles," Biomaterials, vol. 33, no. 33, pp. 8632–8640, 11, 2012. [PubMed: 22922023]

[41]. Chen NT, Wu CY, Chung CY, Hwu Y, Cheng SH, Mou CY, and Lo LW, "Probing the dynamics of doxorubicin-DNA intercalation during the initial activation of apoptosis by fluorescence lifetime imaging microscopy (FLIM)," PLoS One, vol. 7, no. 9, pp. e44947, 2012. [PubMed: 23028696]

[42]. Choukroun GJ, Marshansky V, Gustafson CE, McKee M, Hajjar RJ, Rosenzweig A, Brown D, and Bonventre JV, "Cytosolic phospholipase A(2) regulates Golgi/ER structure and modulates intracellular trafficking of membrane proteins," J Clin Invest, vol. 106, no. 8, pp. 983–93, 10, 2000. [PubMed: 11032858]

[43]. Alberts B, Molecular biology of the cell: The lipid bilayer, 4th ed., New York: Garland Science, 2002.

[44]. Leslie CC, Gangelhoff TA, and Gelb MH, "Localization and function of cytosolic phospholipase A2alpha at the Golgi/ER," Biochimie, vol. 92, no. 6, pp. 620–6, 6, 2010. [PubMed: 20226226]

[45]. Gorini S, De Angelis A, Berrino L, Malara N, Rosano G, and Ferraro E, "Chemotherapeutic drugs and mitochondrial dysfunction: focus on doxorubicin, trastuzumab, and sunitinib," Oxid Med Cell Longev, vol. 2018, pp. 7582730, 2018. [PubMed: 29743983]

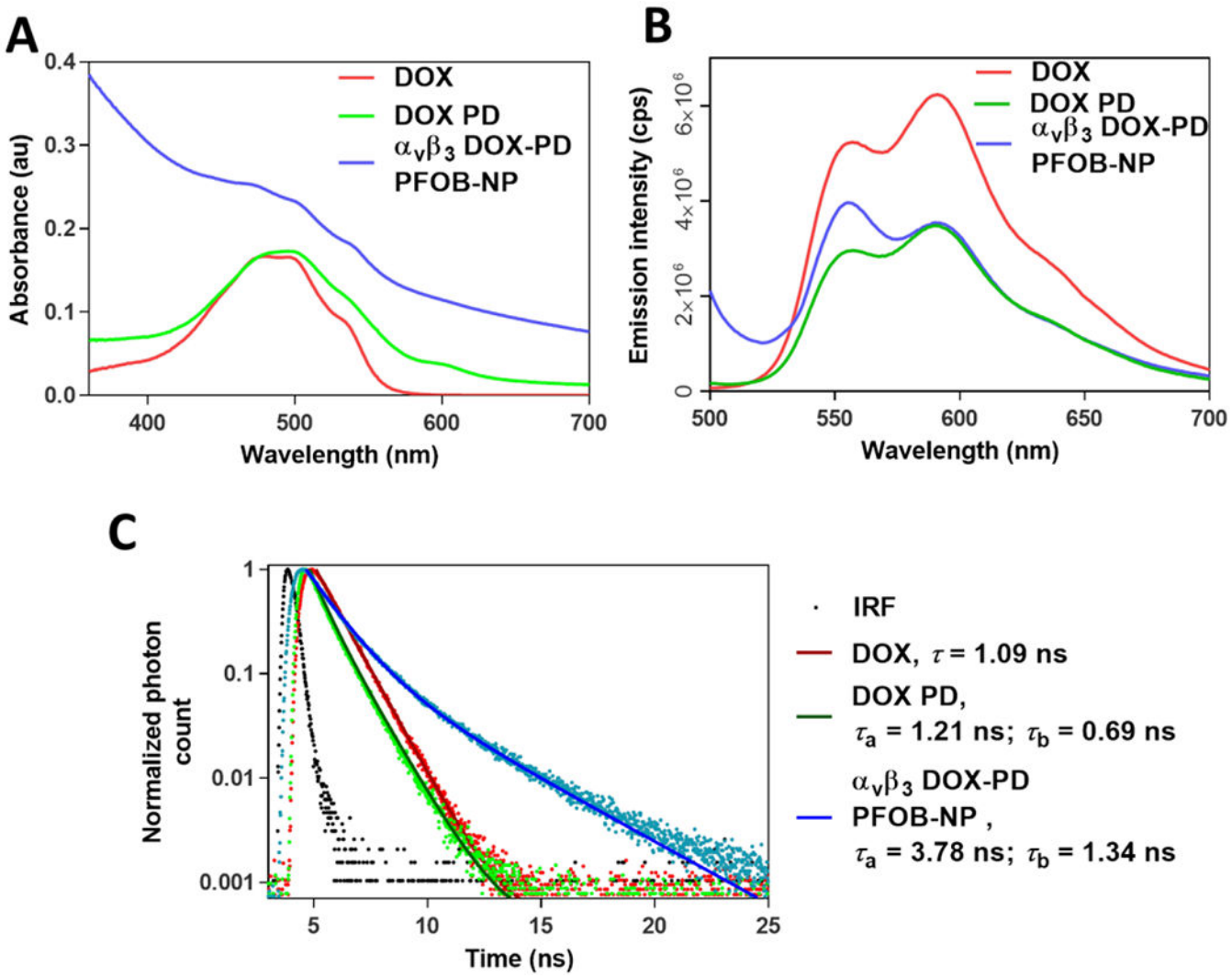

Figure 1.

Spectroscopic characterization of doxorubicin (DOX), doxorubicin prodrug (DOX PD), and αvβ3-integrin targeted prodrug nanoparticles (αvβ3-DOX-PD PFOB-NPs) in water: Absorption spectra of the materials (A). The absorption of doxorubicin prodrug in nanoparticle formulation is obscured by light scattering. Presence of doxorubicin is confirmed in the corresponding fluorescence emission (B). Fluorescence decay characteristics of the materials (C). DOX decay can fit to mono-exponential decay of 1.09 ± 0.02 ns. DOX-PD can fit to bi-exponential decay with τ_a = 1.21 ns (47%); τ_b = 0.69 ns (53%). DOX-PD NP can fit to bi-exponential decay with τ_a = 3.78 ns (22%); τ_b = 1.34 ns (78%). Data represent mean ± sd, n=3 measurements. IRF – Instrument response function.

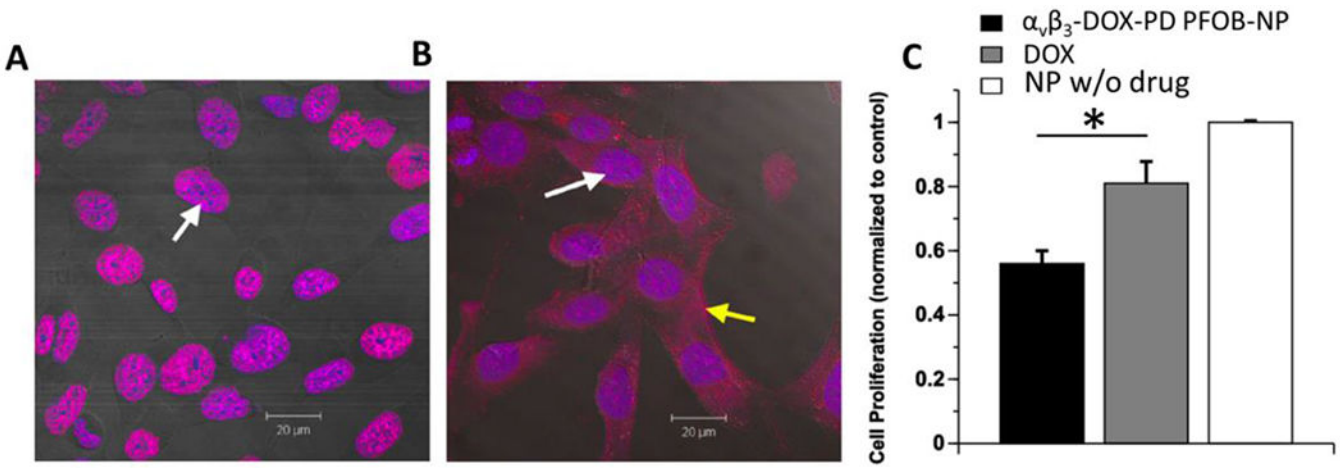

Figure 2.

Cellular internalization and cytotoxic effects of αvβ3-DOX-PD PFOB-NP: Internalization of DOX and αvβ3-DOX-PD PFOB-NP in 2F2B cells incubated with reagents for 30 min. Red shows doxorubicin fluorescence signal and blue is nuclear counterstain, overlay is purple. (A) 2F2B cells treated with free DOX showing most red signal localized into nucleus (white arrow). (B) 2F2B cells treated with αvβ3-DOX-PD PFOB-NP showing signal diffuse through cytosol, membrane (yellow arrow) and nucleus (white arrow). (C) MTT cytotoxicity assay after 48 h of treatment, showing αvβ3-DOX-PD PFOB-NP was significantly more cytotoxic than the equivalent dose of free DOX ($p<0.05$) while drug-free NP had no effect on cell proliferation. Statistical analysis was performed using unpaired Student's T test and p values were assigned.

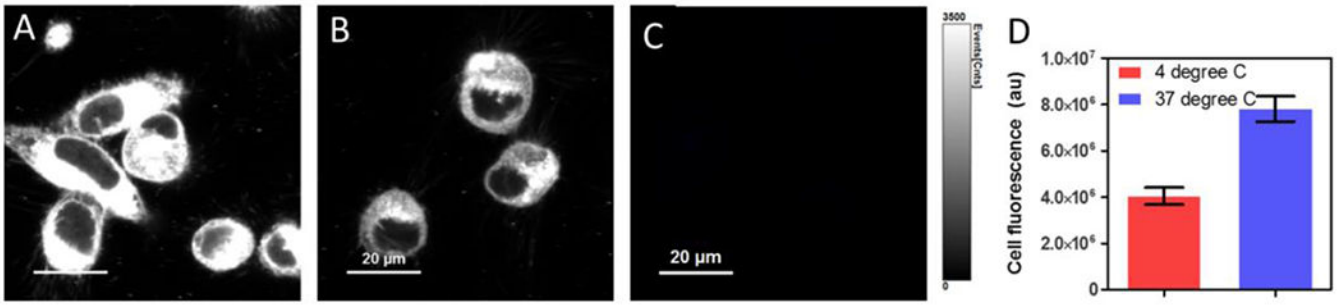

Figure 3.

Effect of temperature on cellular uptake of αvβ3-DOX-PD PFOB-NP: Comparison of cellular uptake of αvβ3-DOX-PD PFOB-NP after 1 h incubation at 37 degrees (A) and 4 degrees C (B). Control untreated cells show near zero signal (C). Quantified background corrected whole cell fluorescence (mean ± sem, n=5 cells for each of the 3 independent experiments) showing internalization is reduced at 4 degrees C (D).

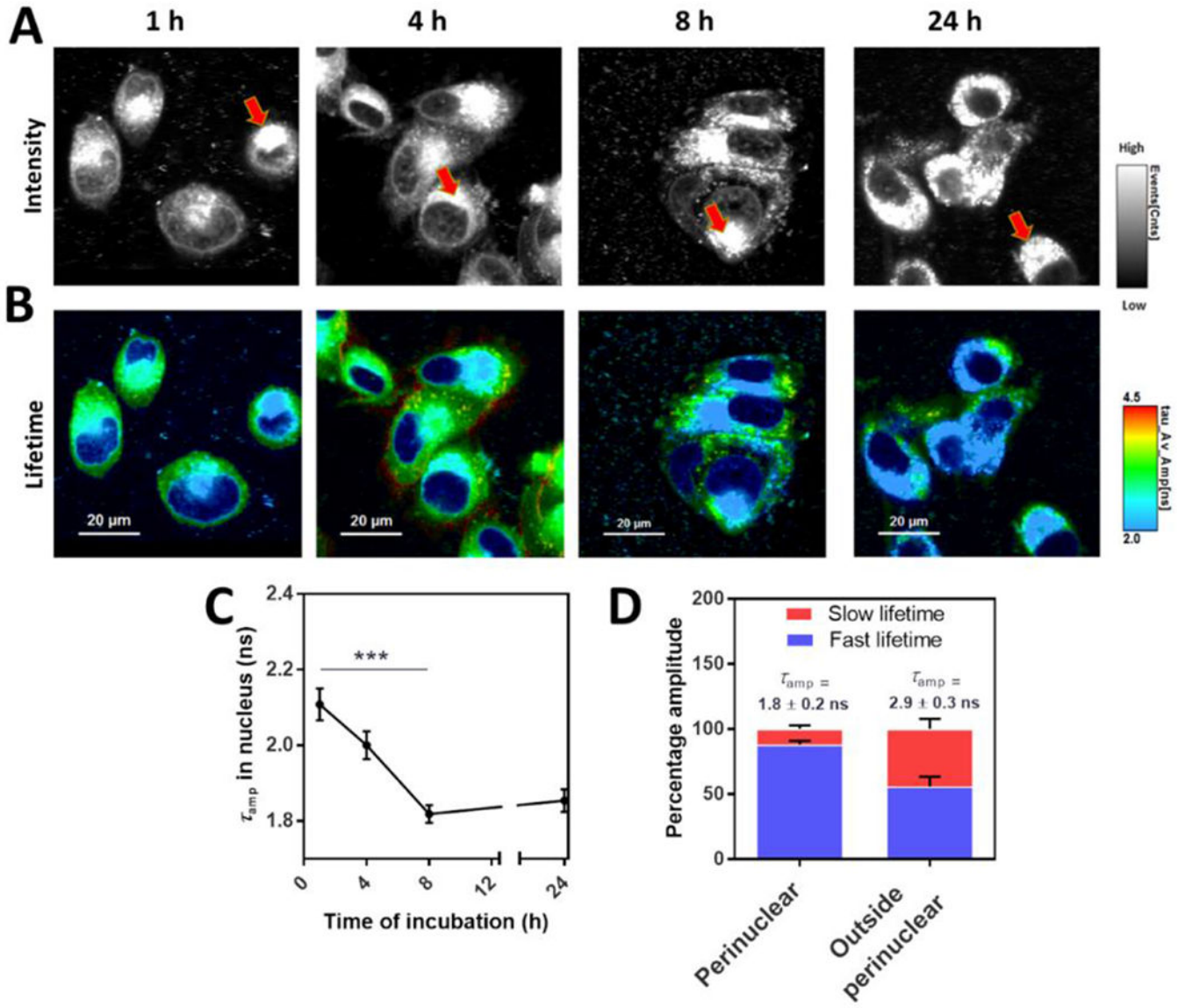

Figure 4.

Fluorescence lifetime imaging of C-32 cells treated with αvβ3-D0X-PD PFOB-NP. Fluorescence intensity images of C-32 cells with αvβ3-DOX-PD PFOB-NP for 1, 4, 8, and 24 h, showing doxorubicin fluorescence from cell cytoplasm and nucleus at all time points. A perinuclear space with high signal intensity is observed in all cells (red arrows) indicating accumulation of drug (A). Corresponding fluorescence lifetime images generated by pixel-by-pixel fitting of decay data show a gradient of τ_{amp} in different cell compartments (B). Quantification of τ_{amp} from nuclear compartments shows time dependent decrease (n= 7-18 cell nuclei at each time point, 3 independent experiments, $p<0.001$) suggested drug induced apoptosis (C). Percentage contributions of slow and fast components in the bright perinuclear region (τ_{amp} = 1.8 ± 0.2 ns) compared to the rest of the cytosol ((τ_{amp} = 2.9 ± 0.3 ns)) for cells treated with αvβ3-DOX-PD PFOB-NP for 8 h (D). Bright perinuclear ROIs show greater contribution of fast lifetime than cytosolic regions outside it (mean ±

sem, n= 15 cell ROI measurements). Statistical analysis was performed using unpaired Student's T test and statistical significance was assigned for $p<0.001$, represented by ***.

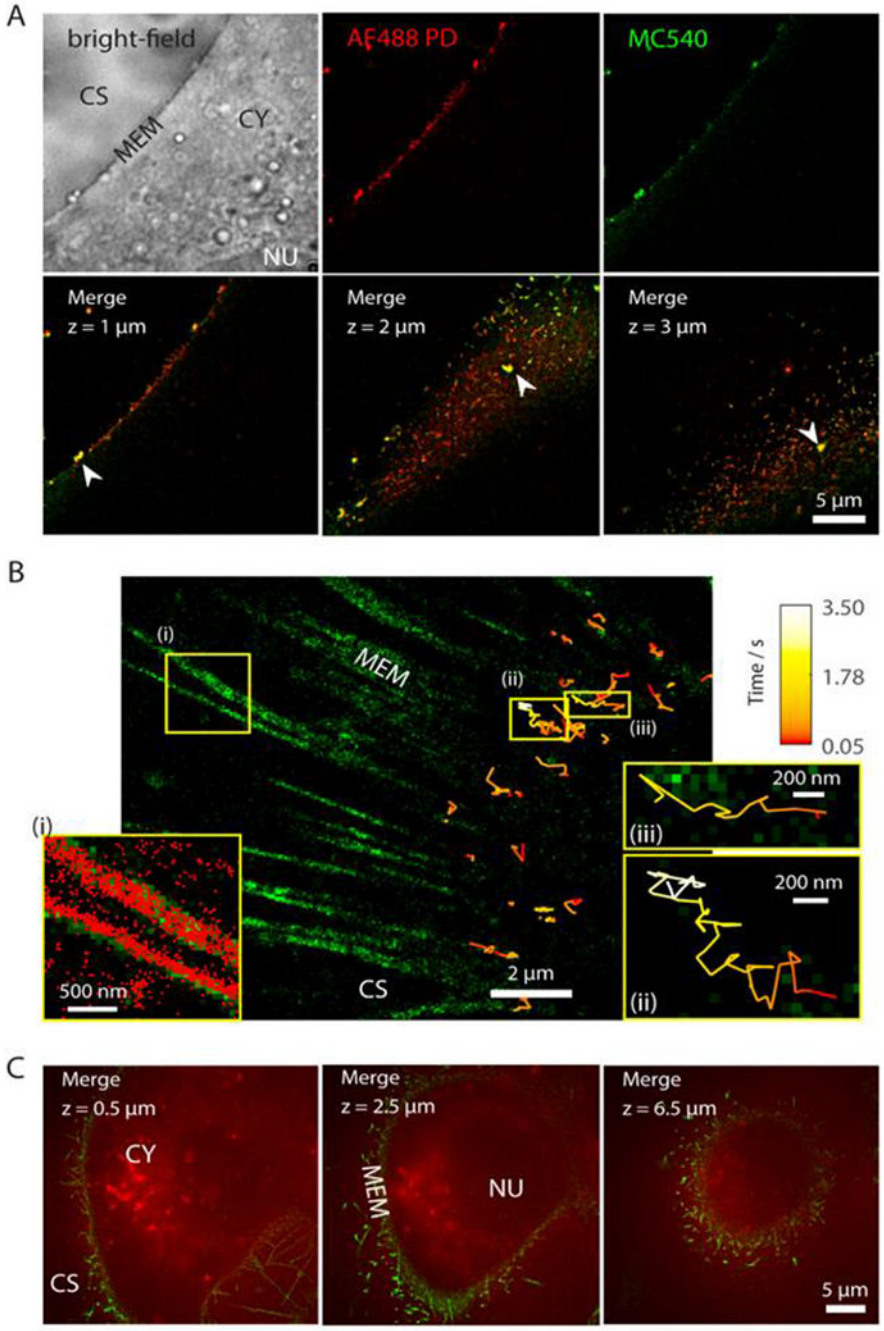

Figure 5.

Early-stage binding of AF488-PD on the membrane and internalization in 2F2B cells. (A) Bright-field and super-resolution images of AF488-PD (red, after 5 min incubation) and cell membrane probe MC540 (green) on the membrane of a 2F2B cell. The overlay images are focused at different heights above the coverslip. The arrows indicate the colocalized active binding sites of AF488-PD and MC540 on the membrane. (B) Both transient binding and diffusion (trajectories on the right part of the image) of single AF488-PD molecules were observed on the cell membrane after 5 min incubation. Trajectories on the filopodia were not

shown. Magnified views of the boxed regions shown in insets: (i) scatter plot of single AF488-PD molecules (red) binding to filopodia, (ii, iii) representative trajectories of single AF488-PD molecule diffusing on the cell membrane with the total length of 3.50 s and 1.65 s, respectively; color-coded for time. (C) Fluorescence images of AF488-PD (red) after a 12-hour incubation at different heights above the coverslip, showing intracellular accumulation of the prodrug. PAINT images of MC540 (green) indicate the contour of the cell membrane. CS, coverslip; MEM, membrane; CY, cytoplasm; NU, nucleus.